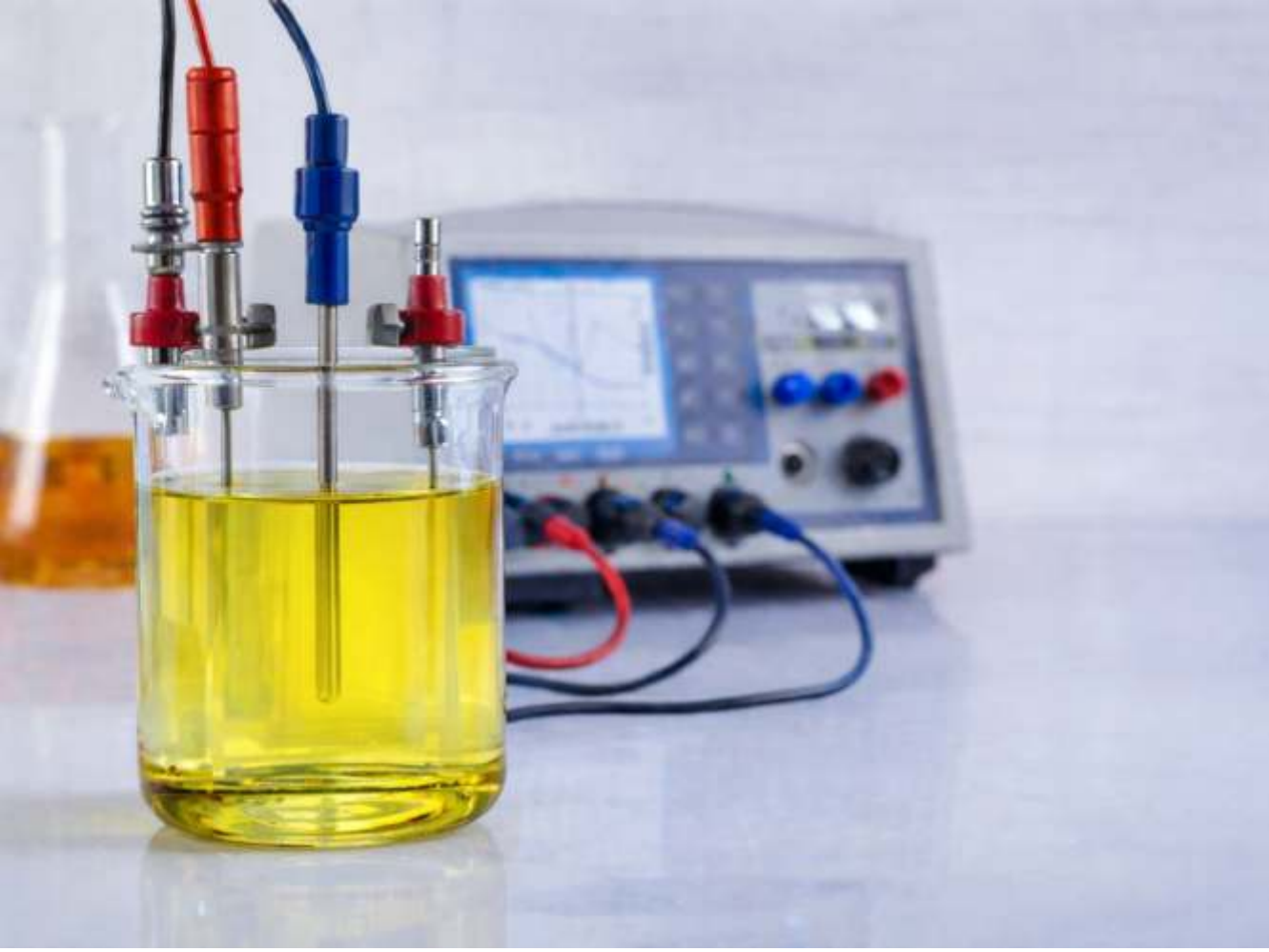

The Use of Thiourea as Corrosion Inhibitor for Super Duplex Stainless Steel in Hydrochloric Acid Solution

Ailton Macedo Medeiros
Fernando B. Mainier
Humberto Nogueira Farneze

DeepScience

The Use of Thiourea as Corrosion Inhibitor for Super Duplex Stainless Steel in Hydrochloric Acid Solution

Ailton Macedo Medeiros

Universidade Federal Fluminense, Niterói, Rio de Janeiro, Brazil

Fernando B. Mainier

Universidade Federal Fluminense, Niterói, Rio de Janeiro, Brazil

Humberto Nogueira Farneze

Centro Federal de Educação Tecnológica Celso Suckow da Fonseca (CEFET-RJ), Rio de Janeiro, Brazil

DeepScience

Published, marketed, and distributed by:

Deep Science Publishing, 2026
USA | UK | India | Turkey
Reg. No. MH-33-0658412
www.deepscienceresearch.com
editor@deepscienceresearch.com
WhatsApp: +91 7977171947

ISBN: 978-93-7185-783-3

E-ISBN: 978-93-7185-980-6

https://doi.org/10.70593/978-93-7185-980-6

Citation: Medeiros, A. M., Mainier, F. B., & Farneze, H. N. (2026). *The Use of Thiourea as Corrosion Inhibitor for Super Duplex Stainless Steel in Hydrochloric Acid Solution*. Deep Science Publishing. https://doi.org/10.70593/978-93-7185-980-6

Preface

The global market for duplex stainless steels is on the rise, driven by various industrial sectors, and is expected to reach US$2.88 billion by 2028. Recently, there has been a significant increase in the use of new alloys, special coatings, and new corrosion inhibitor formulations in oil and gas production. Duplex and super duplex stainless steel have stood out in the manufacture of special valves, fittings, flanges, and other components, replacing traditional carbon steel. Given these applications, duplex stainless steels are critical to this technological area.

Based on this scenario, this book offers knowledge of the corrosive effects on super duplex stainless alloys, especially in acidic environments. The purpose of this research is to analyze the corrosion resistance of UNS S32760 super duplex stainless-steel coupons in hydrochloric acid with and without a thiourea-based organic corrosion inhibitor to simulate conditions in the oil and natural gas industry. Gravimetric tests showed that adding thiourea significantly reduced the mass loss of the coupons, particularly in solutions with higher thiourea concentrations. Electrochemical analyses confirmed the results of the gravimetric tests, showing that the corrosion rates were within the low corrosivity parameters established by the NACE SP-0775 standard.

Keywords: Super Duplex Stainless Steel, Corrosion Inhibitors, Thiourea, Hydrochloric Acid.

Ailton Macedo Medeiros
Fernando B. Mainier
Humberto Nogueira Farneze

Table of Contents

Deep Science Publishing, 2026
https://doi.org/10.70593/978-93-7185-980-6

DeepScience
Open Access Books

Chapter 1: Introduction

Corrosion is an electrochemical phenomenon that affects the integrity of structures, equipment and industrial systems made of ferrous alloys, including stainless steels [1, 2].

These alloys, including duplex and super duplex stainless steels, are not completely immune to corrosive effects, especially in aggressive environments such as the acid stimulation (acidizing) of reservoir rocks, where acidic solutions such as HCl are injected to increase the permeability of the rock to optimize the extraction of fossil fuels [3-7].

Figure 1 shows a simplified scheme of acid stimulation of an onshore oil well, with three points highlighted. These are the production tubing, which is made of carbon steel; the reservoir rock, which is essentially composed of a carbonate matrix ($CaCO_3$); and the main objective of this study, which is to evaluate the performance of the super duplex stainless steel used in the manufacture of some valves, fittings and specific tools located inside the production tubing and exposed to continuous injection of hydrochloric acid for a given injection period.

The acid solution is injected to dissolve part of the rock (at a pressure lower than the renewal pressure of the reservoir rock), creating conductive channels called "wormholes". These facilitate the flow of oil, natural gas, and formation water from the reservoir rock to the well [3-7].

The dissolution of the rock consisting of $CaCO_3$ with hydrochloric acid can be expressed by the formation of soluble calcium chloride ($CaCl_2$) and the release of carbon dioxide (CO_2) as shown in the reaction:

$$CaCO_3 + 2\ HCl \rightarrow CaCl_2 + CO_2 + H_2O.$$

It is a fact that the electrochemical reactions (anodic and cathodic reactions) resulting from the action of hydrochloric acid on carbon steel (Fe) presented below are intense and favored by the increase in acid concentration and temperature:

Anodic reaction: $Fe - 2\ e^- \rightarrow Fe^{2+}$;

Cathodic reaction: $2\ H^+ + 2\ e^- \rightarrow H_2$;

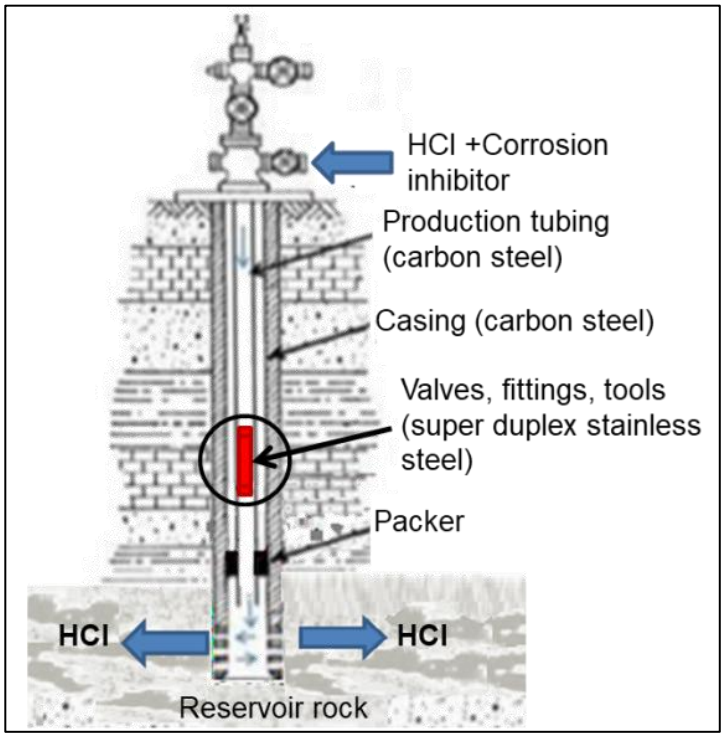

Fig. 1. Hydrochloric acid injection scheme

Despite the existence of multiple strategies to mitigate corrosion, the existing level of control over the said phenomenon could still use improvement, and the number of applicable corrosive processes, ranging between 20 and 30, is still comparatively small, which explains why the current research and the identification of more effective strategies should continue to be further studied.

The adsorption type of corrosion inhibitors mixed in hydrochloric acid is used to film the metal surface and blocking or postponing both the cathodic and anodic reactions.

Conversely, thiourea (CH_4N_2S) has been found to be an effective corrosion inhibitor with immense opportunities in acidic/corrosive conditions largely because of the adsorption process on the metal surface and thus has this direct effect of reducing the rate of corrosion of the carbon steels in the hydrochloric acid solution. [8-11].

In view of the above, the objectives of the following chapters are to evaluate the mechanical and microstructural properties of UNS S32760 super duplex stainless steel coupons, as well as their corrosion processes when immersed in HCl solutions with and without the addition of the corrosion inhibitor thiourea (CH_4N_2S). This evaluation aims

to understand the corrosion inhibition of thiourea in exposed pipe parts under typical working conditions in the oil and gas industry.

Deep Science Publishing, 2026
https://doi.org/10.70593/978-93-7185-980-6

DeepScience
Open Access Books

Chapter 2: Occurrences of mineral scale in pipes and equipment during production in oil wells.

Scale and adherent deposits are common problems in the petroleum industry worldwide. In general, incrustations are defined as any inorganic and/or organic material, or a mixture of the two, that adheres to the walls of pipes and/or equipment. These deposits usually originate from salts present in formation water from reservoir rock. They can cause a partial or total loss of production flow, resulting in losses due to inoperable oil wells and extra operating costs for intervention and cleaning.

As shown in Figure 1, incrustations can occur in pipes, the annular of sand containment screens (gravel pack), subsurface equipment (e.g., valves and pumps), surface equipment (e.g., separator vessels and tanks), and water reinjection systems in oil wells. Figures 2 and 3 show samples of pipes whose internal diameters have been reduced due to the deposition of calcareous scale.

Fig. 2. Example of calcareous scale with reduced internal diameter

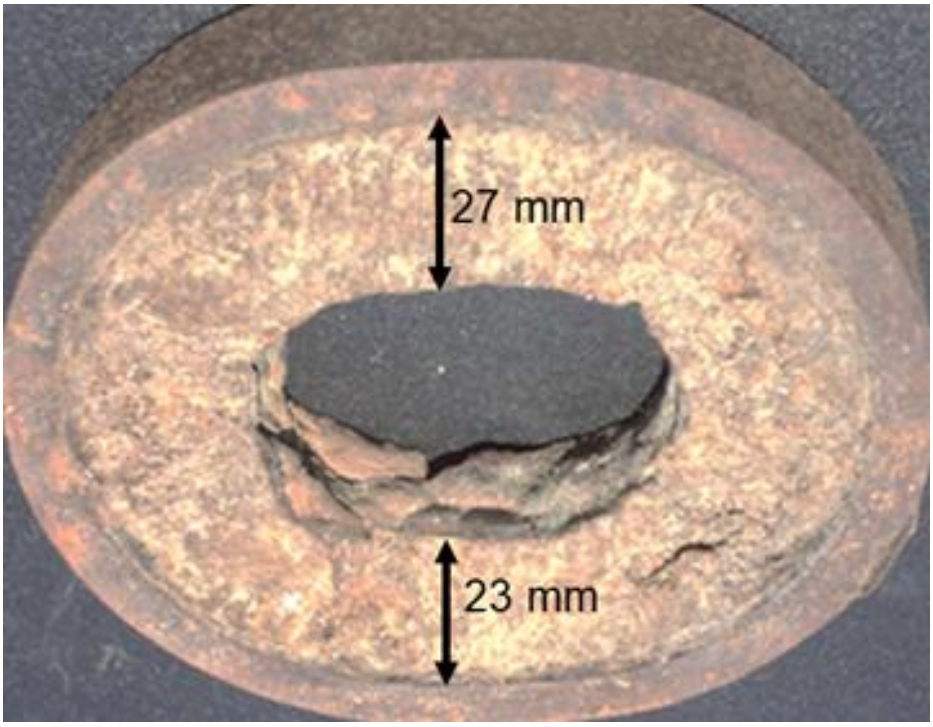

Fig.3 . Horizontal separator tube scale

Once an oil well has exhausted its natural energy, it becomes necessary to use a secondary recovery method. This method commonly involves injecting water (injection water) into the reservoir to displace the oil from the rock's pores. Initially, the formation water is in chemical equilibrium with the environment. However, when foreign water is injected into the reservoir, it can disturb the natural fluid's state, causing insoluble compounds to precipitate [7,12,13].

Additional factors that contribute to the formation of scale include the physicochemical characteristics of the formation water, the oil-to-water ratio of each well, petroleum properties, the geology of the rocks, and variations in the well's temperature, pH, pressure, and hydrodynamic conditions [3,11].

Acidification of the reservoir rock essentially consists of selecting the oil well, characterizing existing damage to the rock formation through laboratory analysis, determining the acidification technique, designing the treatment, executing it, and evaluating the results. Acidification establishment includes a series of standards and a methodology based on collecting as much information and knowledge as possible.

In general, carbonate reservoir rocks are heterogeneous because they exhibit relative variations in porosity and permeability over short distances. They also have micro- and macro-fractures that complicate the uniform distribution of acid in the carbonates. Acidification can connect and/or initiate these fractures by dissolving the material initially filling the fractures in the rock.

Due to its low cost and low formation of insolubles, hydrochloric acid (HCl) is the most widely used acid for dissolving carbonates. Organic acids with weak ionization react more slowly with rock formations. It is more commonly used at high temperatures where lower reactivity systems are desired, corrosion problems are significant, or there are compatibility issues between mineral rock and the formation water and HCl [3,5].

The reaction of HCl with limestone is of the type:

$$2HCl + CaCO_3 \rightarrow CaCl_2 + H_2O + CO_2$$

In dolomitic rocks ($CaCO_3.MgCO_3$), the reaction is represented by:

$$CaMg(CO_3)_2 + 4HCl \rightarrow CaCl_2 + MgCl_2 + 2H_2O + 2CO_2$$

Additives can be used concomitantly with acids to modify the properties of the treatment, thereby improving applicability and reducing side effects. Chemical compatibility tests are performed on rock formations and acid systems to prevent the production of precipitates and sludge. Acid attack is prevented or reduced by using corrosion inhibitors.

Deep Science Publishing, 2026
https://doi.org/10.70593/978-93-7185-980-6

DeepScience
Open Access Books

Chapter 3: Duplex and Super Duplex Stainless Steels

By the year 2023, the worldwide duplex stainless steel registered US$2.31billion in the market due to the industry segments which include pulp and paper, oil and natural gas. It is estimated that this market will grow to USD 2.88 billion by 2028 and its Compound Annual Growth rate (CAGR) will amount to about 4.5. This expansion has been fueled by the increased demand to have the most corrosion-resistant materials with very high levels of durability [14].

Stainless steel is a high resistance corrosive ferrous alloy (Sanni et al. 15). This has been due to the fact that they are at least 11% of chromium (Cr) in composition. Chromium also reacts with oxygen forming a passive layer of chromium oxide (Cr_2O_3) on the surface of the material. The same source also states the fact that this layer serves as a protective enclosure that keeps the alloy apart of the corrosive surrounding and therefore greatly increases the service life and life of these alloys in different industrial applications where corrosion resistance is a necessity.

Addition of other elements including nickel (Ni), molybdenum (Mo), silicon (Si), titanium (Ti), manganese (Mn), phosphorus (P) and sulfur (S) plays successful roles in the accomplishment of the mechanical property expansions of the stainless steels. Stainless steels may also be categorized by the type of dominance of the phases in the ferrous alloy and include (16,17):

- Austenitic stainless steels (austenite);
- Ferritic stainless steels (ferrite);
- Martensitic stainless steels (martensite);
- Duplex stainless steels (austenite and ferrite);
- Triplex stainless steels (austenite, ferrite and martensite).

According to Alar *et al.* [18], this class of stainless steels has a microstructure that is approximately equivalent in the two phases: ferrite and austenite. Figure 4, obtained from a metallographic assay, illustrates the microstructure of duplex stainless steels in terms of the presence of ferritic (dark), austenitic (light), and deleterious (black, located within ferritic grains) phases.

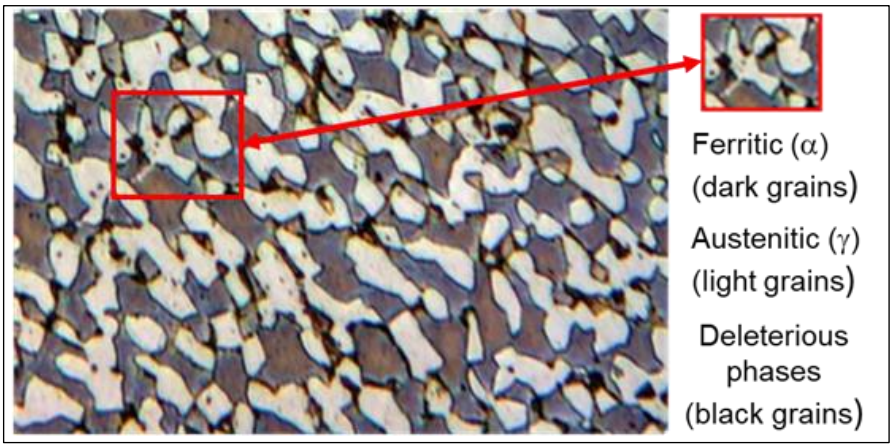

Fig. 4. Microstructure of duplex stainless steel

As previously mentioned, the formation of a microstructure equivalent to the quantitative proportion of ferrite (α) and austenite (γ), as well as the absence of deleterious phases such as intermetallics, nitrides, and carbides, aims to obtain the ideal mechanical strength and corrosion-resistant properties of duplex stainless steels. The recommended treatment to ensure these properties is a controlled cooling and annealing process[19 -23].

Due to their attractive combination of strength, toughness, and excellent corrosion resistance, duplex stainless steels are used in construction, petrochemical, and pulp and paper applications. This can be piping networks to use in cooling systems and heat exchangers, and special type of valves, fittings, flanges, and other elements used in the oil and gas sector and replacing traditional ferrous alloys [24-26].

The description below is a short account of the role that the alloying elements play in the mechanical properties of the duplex stainless steels.

Chromium (Cr): Chromium is a central alloying element in the context of duplex stainless steels, which helps them to be corrosion resistant. It assists in the formation of a passive oxide layer on the material surface how clean it can be resistant to corrosive environments which include saline solutions and marine environments. Chromium also prevents the precipitation of unwanted phases, such as the sigma (σ) phase. The sigma phase significantly compromises the corrosion resistance and toughness of duplex stainless steels under specific conditions, such as prolonged exposure to high temperatures [24,25, 27,28].

Nickel (Ni): Nickel primarily stabilizes the austenitic phase in the microstructure of duplex stainless steels. Depending on the composition of the chemical structure of these alloys, the desired ratio of phases can be regulated, depending on the proportion of ferrite

and austenite, and adding to the optimal mechanical properties tensile strength and pitting resistance ability [29,30].

Molybdenum (Mo), Molybdenum (Mo) is similar to chromium, which directly adds to the anti-corrosion properties of duplex stainless steels by inhibiting the development of damaging intermetallic phases. This renders molybdenum to play an essential role in welding process, as well as, processing of duplex stainless steels [31,32].

According to Jiang et al. [33], duplicates of SN steels have ferrite phase (a) stabilized by elements like chromium (Cr), molybdenum (Mo), silicon (Si), and tungsten (W), and austenite phase (γ) stabilized by including such elements as nickel (Ni), manganese (Mn), carbon (C), nitrogen (N), and copper (Cu). To assert the corresponding stabilization of the ferrite and austenite phases in the form of the microstructure of the duplex stainless steels, the following equations are suggested to the equivalents of chromium: Cr_{equiv} . And Ni_{equiv}.

$$Cr_{equiv.} = \% Cr + \% Mo + 1.5 (\%Si) + 0.5 (\%Nb), \text{ where:}$$

%Cr = percentage of chromium in the alloy;
%Mo = percentage of molybdenum in the alloy;
%Si = percentage of silicon in the alloy;
%Nb = percentage of niobium in the alloy.

$$Ni_{equiv.} = \%Ni + 0.5(\%Mn) + 30 (\%N + \% C), \text{ where:}$$

%Ni = percentage of chromium in the alloy;
%Mo = percentage of manganese in the alloy;
%N = percentage of nitrogen in the alloy;
%C = percentage of carbon in the alloy.

Table 1 below shows the names used by the Unified Numbering System (UNS) and the European Norm (EN) for the main duplex and super duplex stainless steel alloys currently available. It also highlights the alloying elements that make up these alloys and their common and/or commercial names [34].

According to Tanchieva *et al.* [35], the pitting resistance index (PREN) can be used to estimate the resistance to localized corrosion in this class of stainless steels due to the composition rate of Cr, Mo, and N. The value of PREN is obtained through the following equation:

$$PREN = \% Cr + 3.3(\%Mo) + 16(\%N), \text{ where:}$$

%Cr = percentage of chromium in the alloy;
%Mo = percentage of molybdenum in the alloy;
%N = percentage of nitrogen in the alloy.

Duplex alloys with a PREN greater than 40 usually demonstrate extreme resistance to pitting corrosion due to their high chromium, molybdenum, and nitrogen content. These alloys are classified as super duplex stainless steels [35-37].

Table 1 Duplex Stainless Steel/Super Duplex Stainless Steel and their respective alloying elements

				Percentage of the element in the alloy (%)							
Type	**UNS**	**EN**	**Common**	**Cr**	**Ni**	**Mo**	**Cu**	**N**	**Mn**	**Si**	**W**
Lean	S32101	1.4162	2101	21.5	1.5	0.3	0.3	0.22	5	-	-
	S32202	1.4062	2202	22	2	0.3	-	0.2	-	-	-
	S32304	1.4362	2304	24	4	0.3	-	0.1	-	-	-
Standard	S31500	1.4424	3RE60	19	5	2.7	-	0.1	-	1.7	-
	S32900	1.4460	329	25	5	1.5	-	0.1	-	-	-
	S32003	1.4881	2003	22	3.5	1.5	-	0.16	-	-	-
	S31803	1.4462	2205	22	5	3	-	0.17	-	-	-
	S32550	1.4507	255	25	5	3	2	0.15	-	-	-
Super	S32750	1.4410	2507	25	7	4	-	0.28	-	-	-
	S32760	1.4501	Z100	25	7	3.5	0.7	0.24	-	-	0.7
	S32520	1.4507	52N+	25	7	3.5	1	0.25	-	-	-
	S32906	1.4477	2906	25	6	2	-	0.35	-	-	

Source: Adaptation, Alvarez-Armas, & Degallaix-Moreuil, 2013 [34]

The UNS S32760 super duplex stainless steel which has been used in the laboratory experiments in this study most importantly contains considerable percentages of nickel, chromium and molybdenum in terms of its chemical composition. It also has a slight percentage of carbon, manganese, phosphorus, sulfur, silicon, nitrogen, copper, and tungsten. Additionally, it has a density of 7.84 g/cm³. Table 2 illustrates the percentage of the chemical constituents of UNS S32760 super duplex stainless steel based on ASTM A479/A479M (2012) [38].

Table 2 Chemical Composition - UNS S32760 Super Duplex Stainless Steel

Percentage	**Element present in the metal alloy (%)**											
change	C	Mn	P	S	Si	Cr	Ni	N	Mo	Cu	W	Fe
Maximum	-	-	-	-	-	24	6	0.2	3	0.5	0.5	
Minimum	0.03	1	0.03	0.01	1	26	8	0.3	4	1	1	Bal.

Source: Adaptation, ASTM A479/A479M [38],

In addition to the commonly used expression to obtain the PREN, Torres *et al.* [39] report that it can have many versions. Given the presence of element W in the AISI UNS S32760 chemical composition, the PREN index can be calculated using the following expression:

$$PREN_W = \% Cr + 3.3(\%Mo + 0.5\%W) + 16(\%N), \text{ where:}$$

%Cr = percentage of chromium in the alloy;
%Mo = percentage of molybdenum in the alloy
%N = percentage of nitrogen in the alloy;
%W = percentage of tungsten in the alloy.

Like duplex stainless steels, this material has an ideal balance of mechanical strength, ductility, and corrosion resistance due to its equivalent proportions of ferrite (δ) and austenite (γ). The ferrite phase has a high concentration of Cr and Mo and is characterized by its high mechanical strength. The austenite phase has high concentrations of Ni, Mn, and N and is characterized by its toughness and ductility [40].

The treatments necessary to obtain the aforementioned mechanical properties are as follows: the solubilization heat treatment dissolves the phases that precipitate during processing at temperatures below 1050 °C and adjusts the volumetric fractions of the δ and γ phases. The isothermal aging treatment involves heating at a lower temperature, usually between 700 °C and 900 °C, to allow the alloying elements to dissolve in the δ and γ phases, thereby increasing corrosion resistance[40, 42].

However, if care is not taken regarding temperature control during the aging treatment, this material is susceptible to the formation of other secondary phases, such as sigma (σ), chi (χ), chromium nitride (CrN), carbides ($M_{23}C_6$), and secondary austenite (γ2-Fe), which can compromise the material's toughness and corrosion resistance [43].

It is important to highlight that, regarding the requirements of materials and components applied in infrastructures to support oil processing, the Norwegian standard NORSOK M-630 [44] recommends 32 HRC (Hardness Rockwell C) as the maximum acceptable hardness value for connections produced in UNS S32760 super duplex stainless steel, representing, therefore, the reference in terms of hardness for the material studied in this research.

Deep Science Publishing, 2026
https://doi.org/10.70593/978-93-7185-980-6

DeepScience
Open Access Books

Chapter 4: Laboratory experiments with coupons of UNS S32760 super duplex stainless steel

4.1 Chemical Analysis of UNS S32760 Super Duplex Stainless Steel Coupons

A UNS S32760 super duplex stainless steel bar was used for the chemical analysis of the coupons to be used in this study. The results are presented in Table 3 and are in accordance with the ASTM A479/A479M standard [38].

Table 3 Chemical composition of UNS S32760 Super Duplex Stainless Steel (% by mass, Fe in balance)

UNS S32760		Element,%											
		C	Mn	Cr	Ni	Mo	Si	W	Cu	S	P	N	Fe
Coupons		0.03	0.6	24.6	7.2	3.6	0.39	0.6	0.6	0.007	0.007	0.2	Bal.
ASTM A479	Min	--	--	24	6	3	--	--	--	--	--	--	Bal.
	Max	0.03	1	26	8	4	1	1	1	0.01	0.03	0.3	Bal.

4.2 Preparation of coupons for ferritoscopy, hardness testing and spark optical emission spectrometry

To compare the properties of the available material (cast sleeve) with the specifications of UNS S32760 super duplex stainless steel, ferritoscopy, hardness testing, and spark optical emission spectrometry (spark-OES) were first performed, as detailed in sections 4.2.1 through 4.2.3. One specimen (16×8×5mm) was prepared for these tests.

4.2.1 Ferritoscopy

In terms of microstructural characteristics, the specimen was subjected to a ferritoscopic test using a magnetic induction ferritometer (HELMUT FISCHER, model FMP30). The purpose of this test was to determine the percentage of ferrite in the material based on the principle of magnetic permeability.

During the process, the magnetic field generated by a coil interacts with the ferromagnetic phases of the sample, changing the field and producing a voltage proportional to the volumetric fraction of ferrite present in the material.

4.2.2 Hardness test

The tests were conducted using a tabletop Rockwell hardness tester in accordance with standard ASTM E18 [45] procedures for measuring the resistance of a material to penetration, which is determined by the difference between the initial and final loads, expressed on the Rockwell C (HRC) scale.

4.2.3 Spark Optical Emission Spectrometry (Spark-OES) Analysis

Spark optical emission spectrometry (Spark-OES) was performed to compare the results with the chemical composition requirements for UNS S32760 super duplex stainless steel as specified in the ASTM A479/A479M standard [38]. The analysis identified and quantified the material's elements according to the method based on applied electrical discharges to vaporize the material [46]. This process allows element identification based on the light emitted during the test.

4.3 Preparation of coupons for corrosion tests

16 coupons of UNS S32760 super duplex stainless steel were fabricated for gravimetric and electrochemical testing. Machining processes including turning, cutting, filing and drilling were applied. Figure 5 shows the coupon fabrication process and their geometric dimensions. It is important to note that the machining and engraving processes of the coupons were carried out in accordance with the specific requirements established by the NACE SP0775 standard [47] in order to preserve the mechanical and physical properties of the coupons.

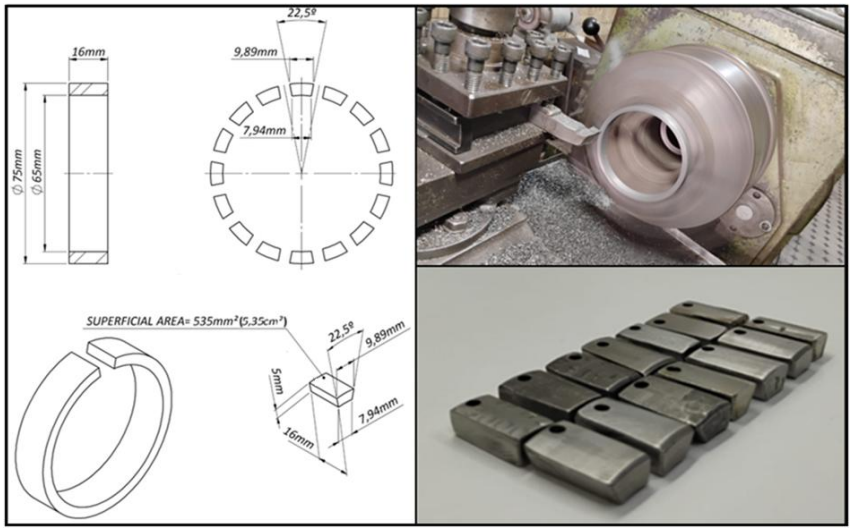

Fig. 5. Making corrosion coupons

4.4 Gravimetric tests (Mass loss)

4.4.1 The Corrosive Medium and Corrosion Inhibitor

The acidic environment which symbolized the corrosion of the limestone rock was 10 percent and 15 percent of the hollow hydrochloric acid. High purity concentrated hydrochloric acid was applicable.

The inhibitor employed was the thiourea corrosion inhibitor which is an organosulfur compound with the following molecular formula (CH_4N_2S). Its structure formula is provided in Figure 6.

Thiourea is a crystalline, white, and bad-smelling organic compound in the form of a crystal that weighs 76.12 g/mol. It dissolves in water and alcohol and fuses at 178 deg C. Its density is 1.406 g/cm³.

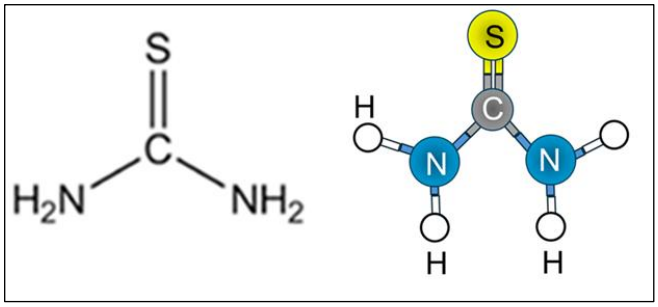

Fig. 6 Molecular structure of the thiourea

Lotus [8] examined the corrosion mechanism of the thiourea and its derivatives. Their study indicates that thiourea as well as the derivatives of thiourea is a potential corrosion inhibitor because of the one sulfur atom and two nitrogen atoms contained in the thiourea molecule. The pair of free electron in these molecules offers the transfer of electrons by the inhibitor to the metal and a covalent bond is formed.

The corrosion inhibitor is used as a protective corrosion inhibitor This is because its adsorption bond is stronger based on the electron density and the donor atom of the functional group and polarization of the group. It is highly adsorbed on metal surfaces gaining a physical barrier and is able to adapt to various contamination conditions and acid concentration conditions. This will enable its usage in diverse corrosive environment and rationalize the safeguarding of stainless steels.

The experiments included placing coupons in 10% and 15% by volume of hydrochloric acid at different temperatures (30°C, 45°C, and 60°C) and with the exposure times of 1 and 3 hours. The design gave a total of 48 different combinations of tests. A total of 96 tests were performed in order to get reliable and accurate results.

Before the gravimetric test, the coupons were sanded using sandpaper 120, 240 and 400 and then washed and wiped down using deionized water and ethyl alcohol, and then dried in the oven to eliminate any residual material.. The initial mass of each coupon was measured using a precision balance (0.1 mg resolution).

From this point, the containers (50 mL Falcon tubes) were filled with 30 mL of solution containing varying concentrations of HCl and thiourea. The coupons were placed in these containers, which were then immersed in a thermostatic bath at 30°C, 45°C, and 60°C for exposure times of 1 and 3 hours. After each test, the cleaning, degreasing, and drying steps were repeated, followed by mass measurement of the coupons to determine mass loss, in accordance with ASTM G31-72 standard [48].

The corrosion rate of the coupons, in terms of mass loss (CR), and the efficiency of thiourea as corrosion inhibitor (E) were defined by the expressions:

$$CR = \frac{W_o - W_i}{S \cdot t} \quad \text{and} \quad E = \left(\frac{W_o - W_i}{W_o}\right) x\ 100, \text{ respectively, where:}$$

W_o and W_i = weight loss in the absence and presence of thiourea (mg);
S = superficial area of the coupons (cm^2);
t = exposure time (h).

4.5 Electrochemical tests (polarization)

The number of tests was determined by a combinatorial analysis of electrolyte solutions, considering thiourea concentrations (250 mL, 500 mL, and 1000 mL) and HCl concentrations (10% and 15% by volume), along with the most unfavorable temperature from the gravimetric tests (60°C), resulting in eight tests. Prior to conducting the polarization tests, the electrolyte solutions were prepared. The working electrodes (WEs) were then prepared by connecting the coupon to a rigid copper wire (2.5 mm^2 cross section).

Each coupon was placed in a segment of PVC tubing, embedded in a mixture of resin and catalyst, and finished with sandpaper of various grits (100-1200) as shown in Figure 7.

Fig. 7. Working electrodes (WE)

The working electrodes (WE), the platinum auxiliary electrode (AE), and the reference electrode (RE) were immersed into a container that was washed to eliminate any dirt and put into the solution of the electrolyte to ensure that none of the electrodes was in contact with the solution. A thermostatic bath was then added to the cell with the electrodes connected to the Potentiostat (AUTOLAB PGSTAT204) to trace the polarization curves that were made potential dynamic polarization tests after varying the potentials in a 60 m V/min steps between -300 mV and +300 mV at a common open circuit potential. In Figures 8 and 9, the major steps of such a process are presented.

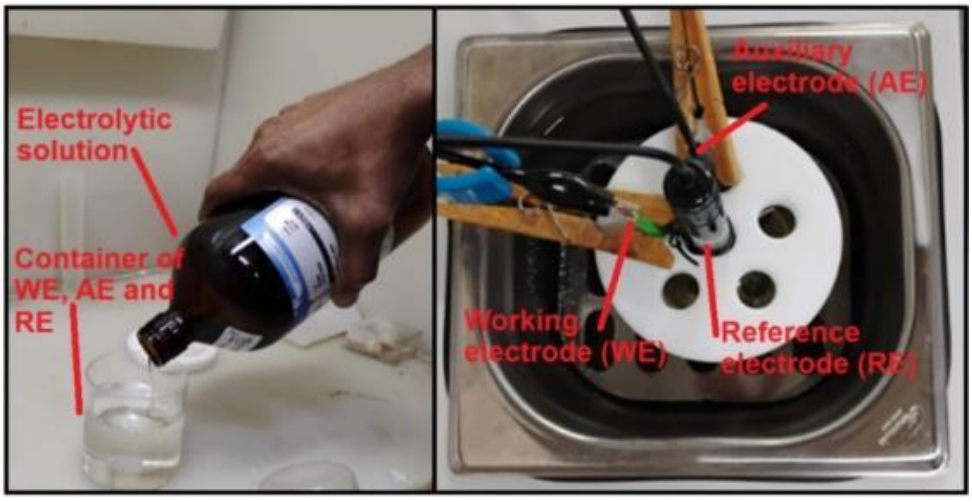

Fig. 8. Electrode cell preparation

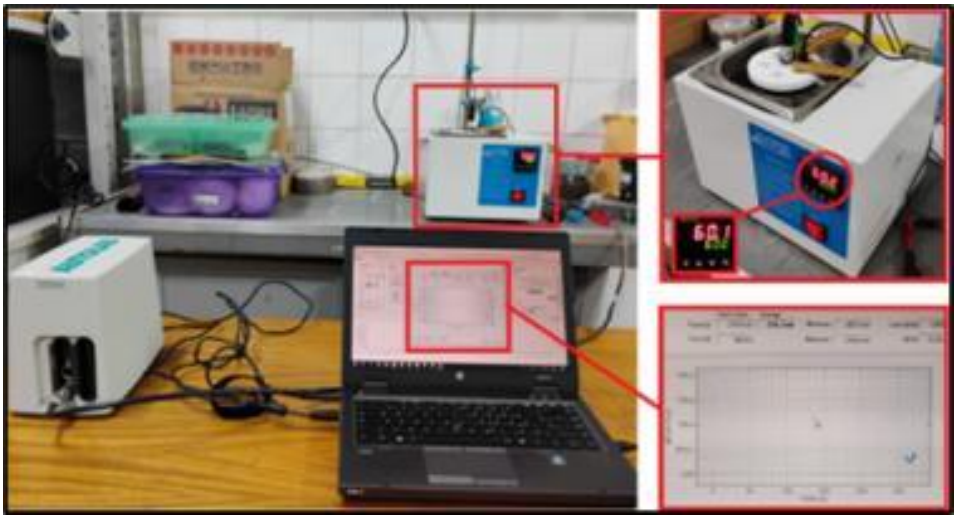

Fig. 9. Electrochemical cell assembly

Placing electrochemical cell together had initially, the working electrode (WE) in each of the electrochemical tests being stabilized and hence the leveling of the anodic and cathodic currents. This was then accompanied by the commencement of potentiodynamic polarization cycle and this yielded polarization curves (extrapolation of the Tafel lines).

From the results, the corrosion rate in terms of penetration (CRp) was determined by the expression:

$$CR_P = \frac{K \cdot i_{corr} \cdot EW}{\rho}$$

as outlined by ASTM G102 standard [49], where:

K = conversion constant (3.27×10^{-3} mm.g / µA.cm².year);
i_{corr} = corrosion current density (µA /cm²);
EW = equivalent weight;
ρ = material density = 7.84 g/cm³ for UNS S32760 super duplex stainless steel.

Regarding the UNS S32760 super duplex stainless steel equivalent weight, it was obtained through the expression

$$EW = \frac{1}{\sum \frac{n_i \cdot f_i}{W_i}}$$

where:
EW = equivalent mass of the metal alloy;

n_i = valence of the infinite element of the metal alloy;
f_i = mass fraction of the infinite element in the metal alloy;
W_i = atomic mass of the infinite element in the metal alloy.

Finally, after obtaining the corrosion rates from the tests, the findings can be associated with qualitative corrosivity classifications according to [47], as shown in Table 3. It is worth noting that surface analysis of the equivalent mass of the metal alloy (WE), through a metallurgical microscope, were performed after some of the electrochemical tests in order to identify pitting occurrences.

Once the corrosion rates, expressed in mm/year, were obtained, the findings could be associated with corrosivity classifications, according to NACE SP0775 [47], as shown in Table 4.

Table 4 – Corrosivity classification

Corrosivity classification	
Corrosion rate, mm/y	Corrosivity
<0.025	Low
0.025 - 0.12	Moderate
0.13 – 0.25	High
>0.25	Severe

It is worth noting that surface analyses, using a metallurgical microscope, was performed after some of the electrochemical tests in order to identify pitting occurrences.

Deep Science Publishing, 2026
https://doi.org/10.70593/978-93-7185-980-6

DeepScience
Open Access Books

Chapter 5: Results and Discussion

5.1 Ferritoscopy

As described above, the ferritoscopy test was performed to determine the ferrite percentage of the material used in the gravimetric and electrochemical tests. Using the calculation method described in ASTM E562 [50], an average ferrite composition of 57.74% was obtained, with a confidence interval of ± 0.58% (Table 5), indicating that the austenite composition of this material is approximately 42%.

Table 5. UNS S32760 super duplex stainless steel: Ferrite percentage calculation

UNS S32760 super duplex stainless steel: ferrite percentage		
x_j (%)		
57.40 58.40	Average percentage of ferrite,%	$\bar{X} = \left(\frac{\sum x_i}{n}\right) = \frac{57.4 + 58.4 + 57.4 + 57.6 + 57.4 + \cdots + 58.3}{10} = 57.74\%$
57.40 57.60 59.50 56.70	Standard deviation,%	$S = \sqrt{\frac{\sum(X_i - \bar{X})^2}{n-1}} = \sqrt{\frac{(57.4 - 57.74)^2 + \cdots + (58.3 - 57.74)^2}{10-1}} = 0.81\%$
57.40 57.00 57.70	t = multiplier related to the number of fields examined (10) = 2.262 Confidence Interval,95%	$IC\ (95\%) = t \cdot \frac{S}{\sqrt{n}} = 2{,}262 \cdot \frac{0{,}81\%}{\sqrt{10}} = 0{,}58\%$
58.30	Percentage of ferrite,%	$\bar{X} \pm IC\ (95\%) = 57{,}74 \pm 0{,}58\%$

In view of the above, the ferrite content of this material complies with the acceptance intervals of ASTM A995 [51], which specifies the requirements for austenitic-ferritic stainless steel castings and establishes ferrite fractions between 30% and 60%, supplemented by the volumetric percentage of austenite.

5.2 Hardness test

As described *above*, a hardness test was performed to compare the result with the hardness requirements of the NORSOK M-630 standard [44]. The test yielded an average value of 30 HRC, as shown in Table 4.

Table 6. Specimen hardness x NORSOK M-630 standard

UNS S32760 super duplex stainless steel: hardness (HRC)	
Tested specimen	$H = \frac{H_1 + H_2 + H_3}{n = 3} = \frac{28 + 31 + 28}{3} = 30\ HRC$
NORSOK M-630 standard	≤ 32 HRC

Based on the aforementioned result, the material's hardness (resistance to deformation) aligns with the parameters established by the NORSOK M-630 standard [44], which accepts hardness values up to 32 HRC.

5.3 Pitting Resistance Index ($PREN_W$)

Based on its mechanical properties, chemical composition shown in Table 1, and equivalent ferrite (δ) and austenite (γ) ratios, the UNS S32760 super duplex stainless steel is suitable for use in corrosive chloride-containing environments [41].

Considering these factors, it is possible to evaluate the Pitting Resistance Index (PREN) based on the percentages of chromium, molybdenum and nitrogen using the expression:

$$PREN = \%\ Cr + 3.3(\%Mo) + 16(\%N).$$

Based on the research developed by Torres *et al.* [39, 52] and Haugan *et al*. [53], who considered the presence of tungsten (W) in the chemical composition of this stainless steel, the new Pitting Resistance Index ($PREN_W$) can be calculated based on the expression:

$$PREN_W = \%\ Cr + 3.3\ (\%Mo + 0.5\%W) + 16(\%N)$$

Research in the literature has shown that the presence of tungsten in super duplex stainless steels can improve their performance against pitting and crevice corrosion, although such results are still being debated in the scientific community [52, 53].

The final value of the $PREN_W$ is:

$$PREN_W = 24.63 + 3.3 \times (3.62 + (0.5 \times 0.55) + (16 \times 0.23) = 41.16$$

The literature classifies super duplex stainless steels with a PREN value ≥ 40, indicating that these materials can be very interesting for the oil and gas industry [35, 54, 55].

5.4 Gravimetric Tests (Mass loss)

As it is described in section 4.4.1 the gravimetric tests were conducted through placing the coupons in solutions of the various concentrations of hydrochloric acid (10% and 15% by volume), thiourea (250 mg/L, 500mg/L and 1000mg/L) and temperature (30°C, 45°C and 60°C) and intervals (via 1 hour and 3 hours)..

Following the tests the mass loss (in mg/cm ^{2}) and the corrosion inhibition efficiency of thiourea were obtained as indicated in Figures 10 and 11; Table 7 and Table 8..

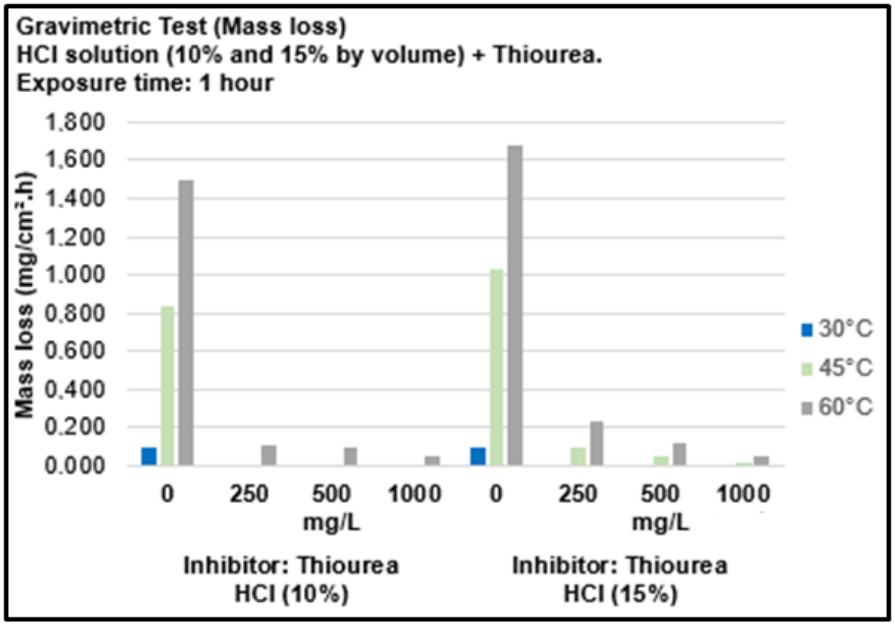

Fig. 10. Corrosion rate (mass loss) in solutions with HCl (10% and 15% by volume), Exposure time: 1 hour

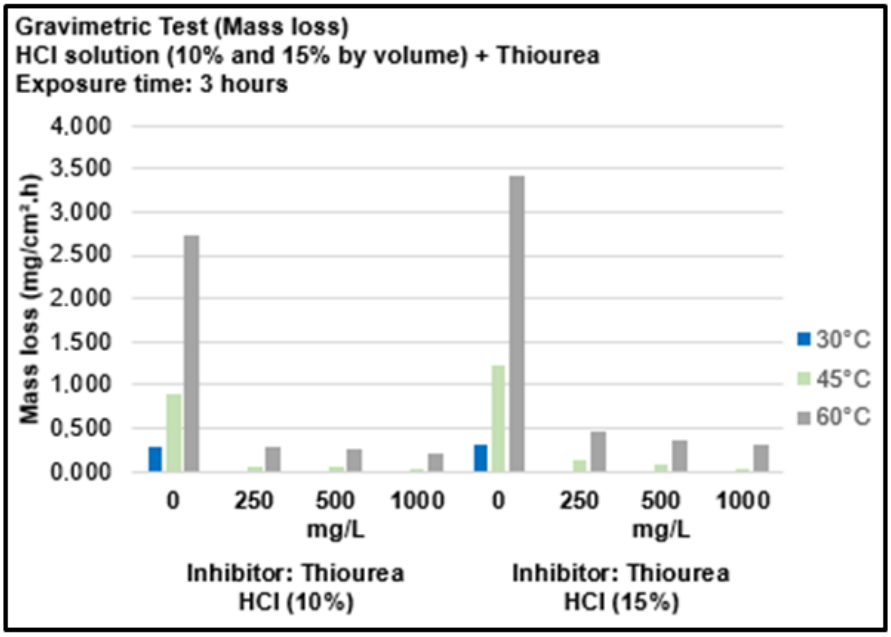

Fig. 11. Corrosion rate (mass loss) in solutions with HCl (10% and 15% by volume), Exposure time: 3 hours

Table 7. Mass loss in HCl solutions (10% and 15% by volume)

		Corrosion Rate – Thiourea (mass loss – mg/cm^2.h)					
		1 hour			3 hours		
HCl	Thiourea	30°C	45°C	60°C	30°C	45°C	60°C
10 %	0	0.094	0.841	1.495	0.280	0.907	2.741
	250 mg/L	0.000	0.000	0.112	0.000	0.062	0.280
	500 mg/L	0.000	0.000	0.094	0.000	0.047	0.249
	1000 mg/L	0.000	0.000	0.047	0.000	0.031	0.218
15 %	0	0.094	1.028	1.682	0.312	1.215	3.427
	250 mg/L	0.000	0.094	0.234	0.000	0.140	0.467
	500 mg/L	0.000	0.047	0.122	0.000	0.094	0.358
	1000 mg/L	0.000	0.019	0.047	0.000	0.041	0.312

Table 8. Efficiency of thiourea in solutions with HCl (10% and 15% by volume)

Corrosion Inhibition efficiency (%)							
		1 hour			3 hours		
HCl	Thiourea	30°C	45°C	60°C	30°C	45°C	60°C
	250 mg/L	100.00	100.00	92.50	100.00	93.10	89.77
10 %	500 mg/L	100.00	100.00	93.71	100.00	94.85	90.91
	1000 mg/L	100.00	100.00	96.88	100.00	96.57	92.05
	250 mg/L	100.00	90.86	86.11	100.00	88.46	86.36
15%	500 mg/L	100.00	95.45	92.75	100.00	92.26	89.55
	1000 mg/L	100.00	98.18	97.22	100.00	96.63	90.91

The gravimetric tests outcomes, both regarding the levels of corrosion rate and the efficiency of thiourea as a corrosion inhibitor to the UNS S32760 super duplex stainless steel are in agreement with the studies of propargyl alcohol-based corrosion inhibitor in stainless steel [56, 57].

The outcome also established the fact that the corrosion protection performance is enhanced with rise in the concentration of thiourea. Moreover, a number of studies have demonstrated carbon steel efficiency by thiourea in different concentrations of HCl. But when the temperature goes beyond 70^{o} C, thiourea may degrade and thereby decrease its corrosion performance [8, 58, 59].

5.5 Electrochemical tests (polarization)

According to the report made above, the polarization curves of UNS S32760 super duplex stainless steel in 60 degC of hydrochloric acid in the presence of thiourea as a corrosion inhibitor was recorded using the AUTOLAB PGSTAT204 Potentiostat.

Figures 12 to 15 are polarization curve of the electrochemical tests with 10 percent (v/v) HCL solution and additions of 250 mg/L, 500 mg/L and 1000mg/L of thiourea whereas, figures 16 to 19 show polarization curves of the electrochemical tests at 15 percent (v/v) HCL solution.

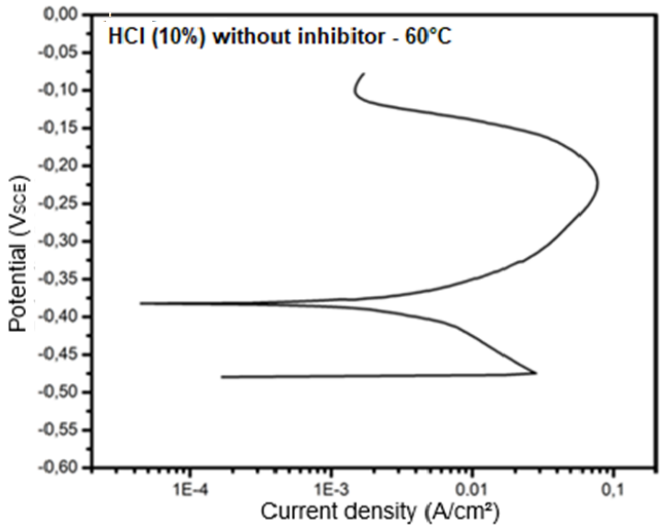

Fig. 12. Potentiodynamic polarization curve: UNS S32760 super duplex stainless steel immersed in HCl solution (10% by volume) without corrosion inhibitor, at 60°C.

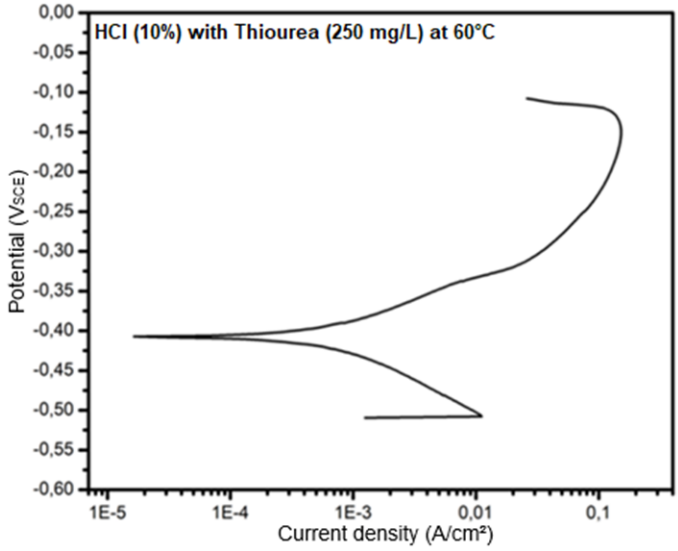

Fig. 13. Potentiodynamic polarization curve: UNS S32760 super duplex stainless steel immersed in HCl solution (10% by volume) with thiourea (250 mg/L), at 60°C

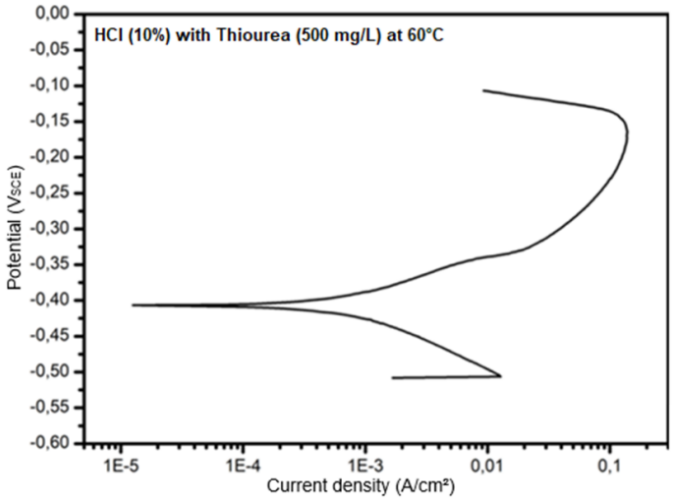

Fig. 14. Potentiodynamic polarization curve: UNS S32760 super duplex stainless steel immersed in HCl solution (10% by volume) with thiourea (500 mg/L), at 60°C

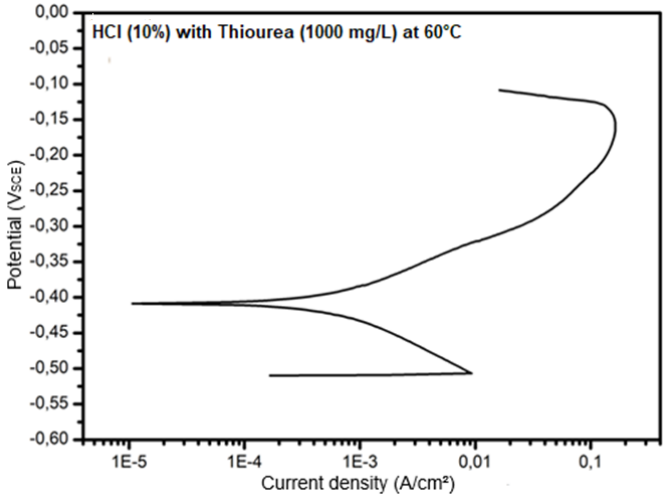

Fig. 15. Potentiodynamic polarization curve: UNS S32760 super duplex stainless steel immersed in HCl solution (10% by volume) with thiourea (1000 mg/L), at 60°C

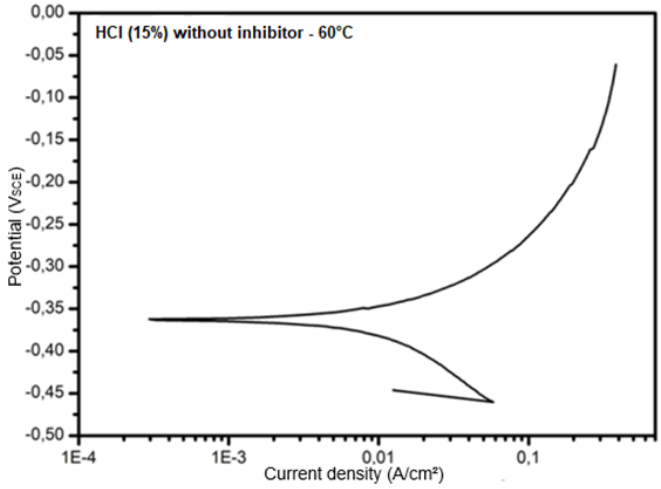

Fig. 16. Potentiodynamic polarization curve: UNS S32760 super duplex stainless steel immersed in HCl solution (15% by volume) without corrosion inhibitor, at 60°C.

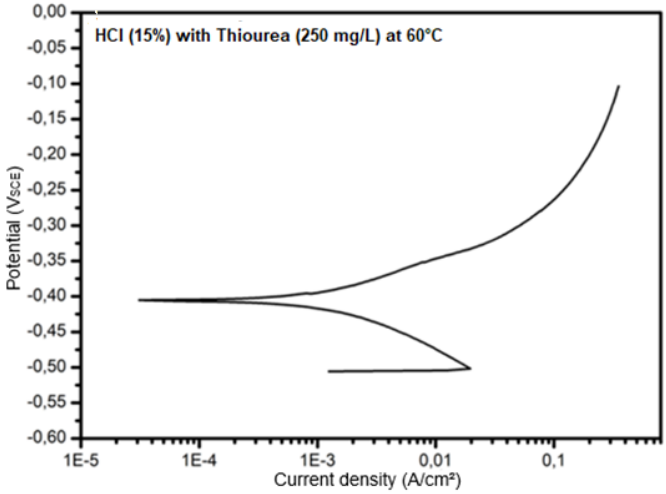

Fig. 17. Potentiodynamic polarization curve: UNS S32760 super duplex stainless steel immersed in HCl solution (15% by volume) with thiourea (250 mg/L), at 60°C

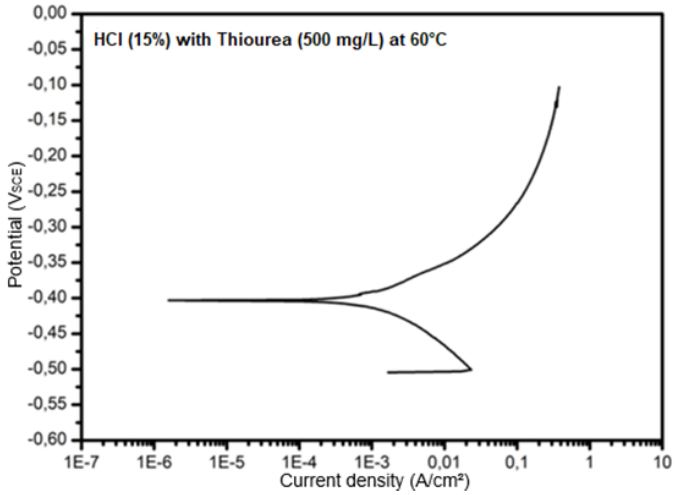

Fig. 18. Potentiodynamic polarization curve: : UNS S32760 super duplex stainless steel immersed in HCl solution (15% by volume) with thiourea (500 mg/L), at 60°C

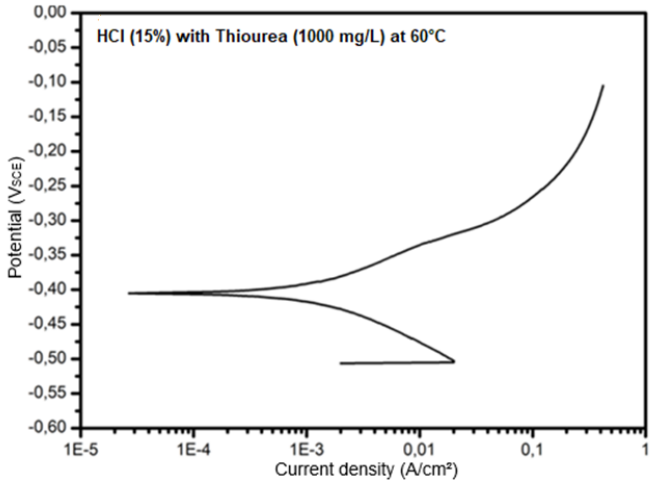

Fig. 19. *Potentiodynamic polarization curve: UNS S32760 super duplex stainless steel immersed in HCl solution (15% by volume) with thiourea (1000 mg/L), at 60°C*

These polarization curves (anodic and cathodic branches) are a first vision that depicts the addition of thiourea to the solution of HCl causes the curves to shift to lower currents and to the same degree, it might be the consequence of an inhibitory effect or the adsorption of a film formed by thiourea molecules on the stainless-steel surface [59].

According to the polarization curves, an acceptable decrease in the anodic and cathodic currents appear in the presence of thiourea against the values of the HCl solution without corrosion inhibitor.

In order to determine the corrosion rates in terms of penetration (CRp) based on the polarization curves (Figures 12 to 19), the equivalent weight of the UNS S32760 super

duplex stainless steel is first determined based on the above and the results are indicated in Table 9.

For the calculation of the equivalent weight (EW) according to ASTM G102 [49], only constituents with a mass fraction greater than 1% (Fe, Cr, Ni, and Mo) were considered.

In addition, the variables needed to calculate the equivalent weight $\mathbf{n_i}$ (valence of the infinite element in the metal alloy), $\mathbf{f_i}$ (mass fraction of the infinite element in the metal alloy), and $\mathbf{W_i}$ (atomic mass of the infinite element in the metal alloy) were obtained from this standard, as well as from the results of the spark OES test and the periodic table provided by the International Union of Pure and Applied Chemistry [44], respectively.

Table 9. Equivalent weight calculation (UNS S32760 super duplex stainless steel)

Equivalent weight (EW)			
Elements	$\mathbf{n_i}$	$\mathbf{f_i}$	$\mathbf{W_i}$
Iron	Fe^{2+}	0.622	55.845
Chromium	Cr^{3+}	0.246	51.996
Nickel	Ni^{2+}	0.072	58.693
Molybdenum	Mo^{2+}	0.036	95.950

$$EW_{UNS\,S32760} = \frac{1}{\frac{n_{Fe} \times f_{Fe}}{W_{Fe}} + \frac{n_{Cr} \times f_{Cr}}{W_{Cr}} + \frac{n_{Ni} \times f_{Ni}}{W_{Ni}} + \frac{n_{Mo} \times f_{Mo}}{W_{Mo}}}$$

$$EW_{UNS\,S32760} = \frac{1}{\frac{2 \times 0.622}{55.845} + \frac{3 \times 0.246}{51.996} + \frac{2 \times 0.072}{58.693} + \frac{2 \times 0.036}{95.950}}$$

$$EW_{UNS\,S32760} = 25.206$$

Table 9 illustrates that the Equivalent weight (EW) of UNS S32760 super duplex stainless steel is 25.206.

The polarization resistance (Rp), corrosion current density (i_{corr}), and potential (E_{corr}) were determined by extrapolating the Tafel lines of the polarization curves of 10% and 15% (v/v) HCl solutions at actual temperatures of 60 C°were determined and are given in Tables 10 and 11.
In addition, these tables show the calculation of the penetration corrosion rate based on the CRp expression according to the ASTM G102 standard [49] and the corrosivity evaluation based on the NACE SP-0775 standard [47].

Table 10. Variables obtained from the polarization curves: HCl (10% by volume) at 60°C

Electrochemical tests(Potentiodynamic polarization) HCl (10 % by volume) at 60°C					
Thiourea mg/L	i_{corr} $\mu A/cm^2$	E_{corr} V	Rp $\Omega.cm^2$	Corrosion rate, mm/y	Corrosivity
0	2.907	-0.392	7.977	0.0306	Moderate
250	0.455	-0.406	31.482	0.0048	Low
500	0.346	-0.402	37.692	0.0036	Low
1000	0.257	-0.411	53.635	0.0027	Low

Table 11. Variables obtained from the polarization curves: HCl (15% by volume) at 60°C

Electrochemical tests(Potentiodynamic polarization) HCl (15 % by volume) at 60°C					
Thiourea mg/L	i_{corr} $\mu A/cm^2$	E_{corr} V	Rp $\Omega.cm^2$	Corrosion rate, mm/y	Corrosivity
0	8.447	-0.363	2.846	0.0888	Moderate
250	0.805	-0.407	16.468	0.0085	Low
500	0.765	-0.404	18.348	0.0080	Low
1000	0.434	-0.405	31.557	0.0049	Low

The potentiodynamic curves and corresponding results show that increasing the inhibitor concentration leads to a decrease in the current density of the system ($\mathbf{i_{corr}}$). This decrease is accompanied by a significant increase in the polarization resistance (**Rp**), indicating an improved protection of the metal surface against corrosion effects.

The behavior of the potentiodynamic curves in response to the corrosive medium (HCl) and the addition of thiourea aligns well with findings from previous studies [61,62].

5.6 Evaluation of the occurrence of pitting on the sample surface after the end of the assays for determining the polarization curves

As shown above, the Pitting Resistance Index ($PREN_W$) for UNS S32760 super duplex stainless steel was 41.16. That is, a value ≥ 40 indicates a low probability of pitting.

In addition, the surfaces of the UNS S32760 super duplex stainless steel electrodes (coupons) exposed to HCl concentrations (10% and 15% by volume) with the addition of 250 mg/L thiourea in the polarization tests were analyzed by light microscopy (Figures 20 and 21) to detect the formation of pits. Based on the 50 μm standard used in the tests, no spots larger than 2.5 μm were observed and based on ASTM G46-21[63].

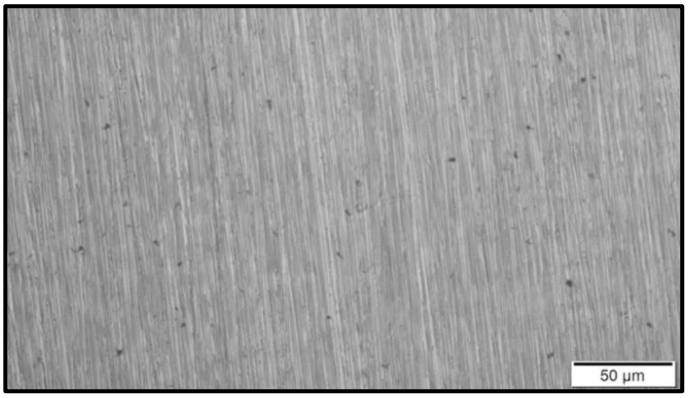

Fig. 20. Optical microscopy: SDSS UNS S32760 immersed in HCl solution (10% by volume) with thiourea (250 mg/L) at 60°C

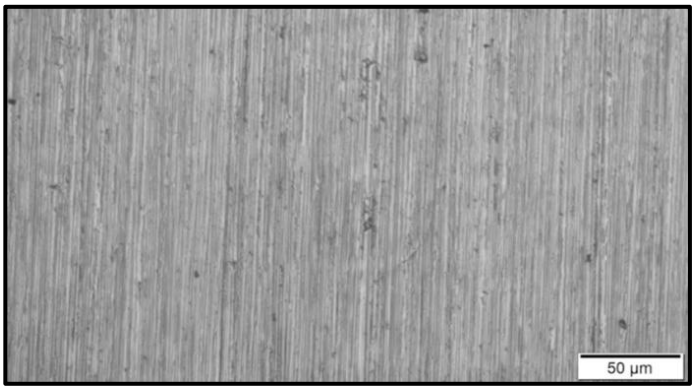

Fig. 21. Optical microscopy: SDSS UNS S32760 immersed in HCl solution (15% by volume) with thiourea (250 mg/L) at 60°C

5.8 Proposed corrosion and corrosion inhibition mechanism

In order to understand thiourea's effect as a corrosion inhibitor for UNS S32760 super duplex stainless steel in HCl solutions, Figure 22 presents the corrosion and protection mechanism proposed in three stages.

The passive films formed in UNS S32760 super duplex stainless steel are ultra-thin, 1 to 3 nm (0.001 to 0.003 µm) thicknesses, and consist of iron, chromium, nickel, molybdenum, and tungsten oxides [64,65]. This passive film can break down under aggressive conditions, causing generalized or localized corrosion damage.

In the first step, without thiourea, the passive film of UNS S32760 super duplex stainless steel partially dissolves in HCl, forming Fe^{3+}, Ni^{2+}, Cr^{3+}, Mo^{4+}, Mn^{2+} and W^{+4} ions that migrate to the acidic medium. Considering that the passive film is ultra-thin, about 0.001 to 0.003 µm, it can be assumed that the concentrations of these formed ions are practically negligible.

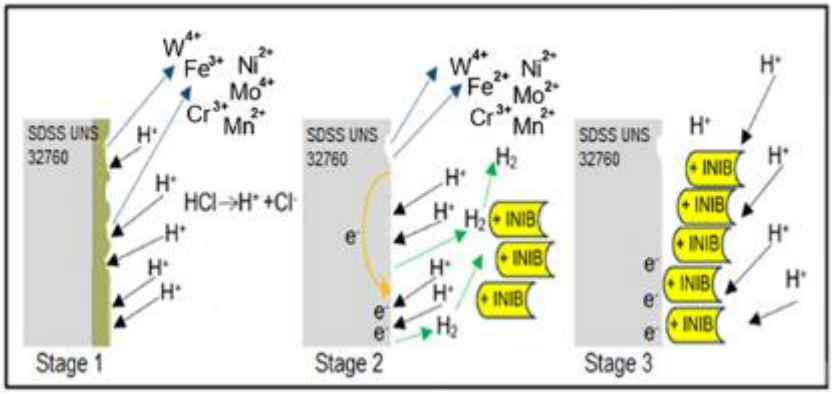

Fig. 22. Proposed corrosion and corrosion inhibition mechanism of UNS S32760 super duplex stainless steel in HCl and in the presence of thiourea

In the second step, it is verified that the passive film has been completely dissolved by HCl, as a result of which the exposed UNS S32760 super duplex stainless steel surface reacts with the hydrochloric acid solution, forming Fe^{2+}, Ni^{2+}, Cr^{3+}, Mo^{4+}, Mn^{2+} and W^{4+} ions.
At the same time, the H^+ ions from the acid solution move to the metal surface (cathodic region), forming atomic hydrogen (H) and then molecular hydrogen (H_2), as described by the anodic and cathodic reactions shown below:

Anodic reactions:
$Fe - 2e \rightarrow Fe^{2+}$
$Ni - 2e \rightarrow Ni^{2+}$
$Cr - 3e \rightarrow Cr^{3+}$
$Mo - 2e \rightarrow Mo^{2+}$
$Mn - 2e \rightarrow Mn^{2+}$
$W - 4e \rightarrow W^{4+}$

Cathodic reaction:
$2H^+ + 2e \rightarrow 2H \rightarrow H_2$

Still in the second stage, the introduction of corrosion inhibitor (thiourea molecules) into the HCl solution causes protonation, as the H^+ ions react partially or completely with the inhibitor molecules, which acquire a positive charge and move towards the cathode.

In the third step, inhibitor molecules adsorb onto the substrate surface and directly prevent H^+ ions from reaching the metal surface and capturing electrons, thereby mitigating corrosive reactions.

Sulfur and nitrogen compounds present in the thiourea molecule promote adsorption on the metal surface, reducing the rate of hydrogen (H_2) evolution [59,66].

It is important to note that this adsorption mechanism was confirmed in electrochemical tests, where the polarization resistance (**Rp**) increased and the corrosion current intensity ($\mathbf{i_{corr}}$) decreased with the addition of thiourea to the electrolyte solutions.

Deep Science Publishing, 2026
https://doi.org/10.70593/978-93-7185-980-6

DeepScience
Open Access Books

Chapter 6: Conclusion

Based on the results of the tests carried out during this research, it can be concluded that:

- The corrosion coupons were made of material that conformed to the characteristics of UNS S32760 super duplex stainless steel in terms of microstructure, mechanical, and chemical properties, as evidenced by the comparison of ferritoscopy, hardness test, and spark OES results to NORSOK M-630, ASTM A479, and ASTM A995 standards, respectively;

- The addition of thiourea significantly reduced corrosion rates. Having incubated thiourea after 3 hours at 30°C in all solutions, the efficiency of thiourea was 100 percent. Efficiencies were 89 to 100 per cent at 45°C and 60°C in 10 per cent HCl and 86 to 98 per cent in 15 per cent HCl solutions;

- Results of electrochemical tests were in agreement with those of gravimetric tests which indicated that corrosion rates of solutions containing thiourea, which is of low corrosivity, as defined by NACE SP-0775. Conversely, the solution that did not include thiourea was moderately corrosive, which is why the presence of the inhibitor is of great significance;

- By using optical microscopy, inclusions (<2.5 μm) which were not connected to corrosion pits were observed. This was corroborated by the pitting resistance index (PREN, 41.16), the adsorption of thiourea and compliance with ASTM G46.

References

[1] Feliciano FF, Leta FR, & Mainier FB. Texture digital analysis for corrosion monitoring. *Corrosion Science*, 2015: 93: 138-147. https://doi.org/10.1016/j.corsci.2015.01.017.

[2] Singh A. Introductory Chapter: Protection of stainless steels in corrosive media. In: Stainless Steels. IntechOpen, 2022, 188. https://doi.org/10.5772/intechopen.106668.

[3] Mainier FB, Alencar Junior AAM, Barros EF. Chemical removal of iron sulfide deposit in pipes from oil and sour gas production. J. Chem. Technol. Metall. 2024; 59(1):165-72. https://doi.org/10.59957/jctm.v59.i1.2024.19.

[4] Boussa M, Bencherif D. Optimization of the producing wells (acidizing-PLT). In: SPE Oklahoma City Oil and Gas Symposium/Production and Operations Symposium; 2003 Mar 23–25; Oklahoma City, Oklahoma. SPE-8091.

[5] Mainier FB, Mainier RJ. Chemical removal of carbonate scale in pipes from oil and gas production. Chem. Mater. Sci. - Dev Innov. BP International, 2024; 4: 119-40. https://doi.org/10.9734/bpi/cmsdi/v4/1053.

[6] Mukhametshin VS. Justification for increasing the performance of hydrochloric acid treatment in wells of fields with carbonate reservoir. IOP Conf Ser Mater Sci Eng. 2020; 905(1):012083. https://doi.org/10.1088/1757-899X/905/1/012083.

[7] Al-Ameri A, Gamadi T. Optimization of acid fracturing for a tight carbonate reservoir. Petroleum. 2020; 6(1):70-9. https://doi.org/10.1016/j.petlm.2019.01.003

[8] Loto RT, Loto CA, & Popoola API. Corrosion inhibition of thiourea and thiadiazole derivatives: a review. J. Mater. Environ. Sci ; 2012 : 3(5), 885-894.

[9] Oliveira CG, Faria VW, Andrade GF, D'Elia E, Cabral MF, Cotrim BA, & Souza FC. Synthesis of thiourea derivatives and its evaluation as corrosion inhibitor for carbon steel. Phosphorus, Sulfur, and Silicon and the Related Elements; 2015: 190(8), 1366-1377. Issue 8: 26 th International Symposium on Organic Chemistry of Sulfur (ISOCS-26).

[10] Shen CB, Wang SG, Yang HY, Long K, & Wang FH. Corrosion and corrosion inhibition by thiourea of bulk nanocrystallized industrial pure iron in dilute HCl solution. *Corrosion Science,* 2006: 48(7), 1655-1665. https://doi.org/10.1016/j.corsci.2005.06.005.

[11] Mainier FB, Freitas AER, and Gonçalves MVS. Corrosion inhibition of thiourea on mild steel in hydrochloric acid contaminated with chlorine. International Journal of Advances in Engineering & Technology. 2020, v. 13, Issue 3, 72-79.

[12] Kamal MS, Hussein I, Mahmoud M, Sultan AS, Saad MA. Oilfield scale formation and chemical removal: A review, *Journal of petroleum science and engineering*, 2018, 171, 127-139. https://doi.org/10.1016/j.petrol.2018.07.037.

[13] Olajire AA. A review of oilfield scale management technology for oil and gas production. *Journal of petroleum science and engineering*. 2015, 135:723-737. https://doi.org/10.1016/j.petrol.2015.09.011.

[14] Mordor intelligence. Duplex stainless steel market. https://www.mordorintelligence.com/pt/industry-reports/duplex-stainless-steel-market.

[15] Sanni O, Sunday Isaac Fayomi O. & Patricia Idowu Popoola, A. Eco-friendly inhibitors for corrosion protection of stainless steel: an overview. In *Journal of physics: conference series,* 2019*,* (Vol. 1378, No. 4, 042047). IOP Publishing. https://doi.org/10.1088/1742-6596/1378/4/042047.

[16] Malandruccolo A. An Introduction to Stainless Steels. In *Superaustenitic Stainless Steels: A Comprehensive Overview*, 2024, 1-71. Cham: Springer Nature Switzerland. https://doi.org/10.1007/978-3-031-68744-0_1.

[17] Luecke WE & Slotwinski JA. Mechanical properties of austenitic stainless steel made by additive manufacturing. *Journal of research of the National Institute of Standards and Technology*, 2014, *119*, 398. https://doi.org/10.6028/jres.119.015.

[18] Alar V, Novak AH, Runje B, & Kurtela M. The effect of $CeCl_3$ inhibitor on the localized corrosion of stainless steel in chloride solutions. *Materials and corrosion*, 2019, *70*(7), 1273-1287. https://doi.org/10.1002/maco.201810509.

[19] Testmat. Detecção de fases intermetálicas em aços inoxidáveis duplex. 2023. https://testmat.com.br/microestrutura/detecao-intermetalicos-inox-duplex/.

[20] Gunn R. (Ed.) *Duplex stainless steels: microstructure, properties and applications*. Elsevier, 1997.

[21] Maki T, Furuhara T, & Tsuzaki K. Microstructure development by thermomechanical processing in duplex stainless steel. *ISIJ Internacional*, 2001, *41*(6), 571-579. https://doi.org/10.2355/isijinternational.41.571.

[22] Tavares SSM, Batista RT, Landim RV, Velasco JAC & Senna LF. Investigation of the effect of low temperature aging on the mechanical properties and susceptibility to sulfide stress corrosion cracking of 22% Cr duplex stainless steel. *Engineering Failure Analysis*, 2020, *113*, 104553. https://doi.org/10.1016/j.engfailanal.2020.104553.

[23] Ho MY, Geddes J, Barmatov E, Crawford L & Hughes T. Effect of composition and microstructure of duplex stainless steel on adsorption behaviour and efficiency of corrosion inhibitors in 4 molar hydrochloric acid. Part I: Standard DSS 2205. *Corrosion Science*, 2018, *137*, 43-52. https://doi.org/10.1016/j.corsci.2018.03.022.

[24] Kahar, SD. Duplex stainless steels-an overview. *International Journal of Engineering Research and Applications*, 2022, *7*(04), 27-36.

[25] Pezzato L. & Calliari I. Advances in duplex stainless steels. *Materials*, 2022, *15*(20), 7132. https://doi.org/10.3390/ma15207132**.**

[26] Dalal M. & Penso J. duplex stainless steel–learning from field experience in oil & gas and petrochemical services. In: *Pressure Vessels and Piping Conference, 2022* , July, (Vol. 86182, p. V04BT06A015). American Society of Mechanical Engineers. https://doi.org/10.1115/PVP2022-84889.

[27] Han Y, Liu ZH, Wu CB, Zhao Y, Zu GQ, Zhu WW. & Ran X. A short review on the role of alloying elements in duplex stainless steels. *Tungsten*, 2023, *5*(4), 419-439. https://doi.org/10.1007/s42864-022-00168-z.

[28] Fedorov A, Zhitenev A, Karasev V, Alkhimenko A, & Kovalev P. Development of a methodology for the quality management of duplex stainless steels. *Materials*, 2022, *15*(17), 6008. https://doi.org/10.1007/s11015-025-01894-8.

[29] Tóth T, Hensel J, Hesse AC. & Dilger K. Electron beam welding of 2205 duplex stainless steel with nickel-based filler wire using multi-beam technique. *Welding in the World*, 2022, *66*(11), 2191-2206. https://doi.org/10.1007/s40194-022-01363-9.

[30] Tóth T, Krasnorutskyi S, Hensel J. & Dilger K. Electron beam welding of 2205 duplex stainless steel using pre-placed nickel-based filler material. *International Journal of Pressure Vessels and Piping*, 2021, *191*, 104354. https://doi.org/10.1016/j.ijpvp.2021.104354.

[31] Paula Inácio LK, Cruz Souza S, Assumpção RF, Souza IR. & Santos DB. Effect of cold rolling and molybdenum content on the kinetics of spinodal decomposition in duplex stainless steels. *Steel research international*, 2025. https://doi.org/10.1002/srin.202500420.

[32] Mutașcu D, Karancsi O, Mitelea I, Crăciunescu CM, Buzdugan D, & Uțu ID. Pulsed TIG cladding of a highly carbon-, chromium-, molybdenum-, niobium-, tungsten-and vanadium-alloyed flux-cored wire electrode on duplex stainless steel X2CrNiMoN 22-5-3. *Materials*, 2033, *16*(13), 4557. https://doi.org/10.3390/ma16134557 .

[33] Jiang Y, Tan H, Wang Z, Hong J, Jiang L, & Li J. Influence of Creq/Nieq on pitting corrosion resistance and mechanical properties of UNS S32304 duplex stainless steel welded joints. *Corrosion Science*, 2013, *70*, 252-259. https://doi.org/10.1016/j.corsci.2013.01.037.

[34] Alvarez-Armas, I., & Degallaix-Moreuil, S. (Eds.). *Duplex stainless steels*. John Wiley & Sons, 2013.

[35] Tahchieva AB, Llorca-Isern N. & Cabrera JM. Duplex and super duplex stainless steels: microstructure and property evolution by surface modification processes. *Metals*, 2019, *9*(3), 347. https://doi.org/10.3390/met9030347.

[36] Francis R. & Byrne G. Duplex stainless steels—alloys for the 21st century. *Metals*, 2023, *11*(5), 836. https://doi.org/10.3390/met11050836.

[37] Fedorov A, Karasev V, Kovalev P, Shaposhniko N. & Zhitenev A. Development of thermodynamic criteria for determining the composition of duplex stainless steels with high corrosion resistance. *Materials*, 2024, *17*(2), 294. https://doi.org/10.3390/ma17020294.

[38] ASTM A479/A479M. American Society of Testing and Materials. Standard specification for stainless steel bars and shapes for use in boilers and other pressure, 2021. West Conshohocken, PA.

[39] Torres C, Johnsen R. & Iannuzzi M. Crevice corrosion of solution annealed 25Cr duplex stainless steels: Effect of W on critical temperatures. *Corrosion Science*, 2021, *178*, 109053. https://doi.org/10.1016/j.corsci.2020.109053.

[40] Lopes B, Rodrigues S, Silva E, Reis G, Martins W, Damascena J. & Leal V. Influence of MIG/MAG welding process on mechanical and pitting corrosion behaviors on the super-duplex stainless steel SAF 2507 welded joints. *Materials Sciences and Applications,* 2018, *9*, 228-245. https://doi.org/10.4236/msa.2018.92015.

[41] Ciuffini AF, Barella S, Di Cecca C, Gruttadauria A, Mombelli D. & Mapelli C. Hot-dip aluminizing on AISI F55–UNS S32760 super duplex stainless steel properties: effect of thermal treatments. *Metals*, 2017, *7*(12), 525. https://doi.org/10.3390/met7120525.

[42] Cojocaru VD, Şerban N, Angelescu ML, Cojocaru EM, Cinca I, Răducanu D. & Vintilă AN. Effect of short duration solution treatment at temperatures below 1000°C on σ-phase precipitation in a super duplex stainless steel alloy: Wirkung einer kurzen lösungsglühdauer bei temperaturen unter 1000°c auf die ausscheidung von σ-phasen in einem super-duplexstahl. *materialwissenschaft und werkstofftechnik*, 2018, *49*(5), 530-537. https://doi.org/10.1002/mawe.201700280.

[43] Khoshnaw F, Marinescu C, Sofronia A, Munteanu C, Marcu M, Barbulescu L E. & Paraschiv A. Microstructural and thermoanalytical characterization of super duplex stainless steel-UNS S32760-F55. *Materials Today Communications*, 2021, *28*, 102644. https://doi.org/10.1016/j.mtcomm.2021.102644.

[44] NORSOK M-630, Norsk Sokkels Konkurranseposisjon. Material data sheets for piping, 2004. Norway.
[45] ASTM E18-17 American Society of Testing and Materials. Standard test methods for rockwell hardness of metallic materials, 2017. West Conshohocken, PA.
[46] Bengtson A. Laser Induced Breakdown Spectroscopy compared with conventional plasma optical emission techniques for the analysis of metals. A review of applications and analytical performance. Spectrochim. Acta Part B At Spectrosc., 2017; v. 134, 123-132 https://doi.org/10.1016/j.sab.2017.05.006.
[47] NACE SP 0775. National Association of Corrosion Engineers. Preparation, installation, analysis and interpretation of corrosion coupons in oilfield operations. 2013. Houston, TX, USA.
[48] ASTM G31-72. American Society of Testing and Materials. Standard practice for laboratory immersion corrosion testing of metals, 2004. West Conshohocken, PA.
[49] ASTM G102-23. American Society of Testing and Materials. Standard practice for calculation of corrosion rates and related information from eletrochemical measurements, 2023. West Conshohocken, PA
[50] ASTM E562-11. American Society of Testing and Materials. Standard test method for determining volume fraction by systematic manual point count, 2011. West Conshohocken, PA.
[51] ASTM A995/A995M. American Society of Testing and Materials. Standard specification for castings, austenitic-ferritic (duplex) stainless steel, for pressure-containing parts, 2011. West Conshohocken, PA.
[52] Torres C, Hazarabedian MS, Quadir Z, Johnsen R, & Iannuzzi M. The role of tungsten on the phase transformation kinetics and its correlation with the localized corrosion resistance of 25Cr super duplex stainless steels. J. Electrochem. Soc.; 2020, 167(8), 081510. https://doi.org/10.1149/1945-7111/ab90af, 081510.
[53] Haugan EB, Næss M, Rodriguez CT, Johnsen R, & Iannuzzi M. Effect of tungsten on the pitting and crevice corrosion resistance of type 25Cr super duplex stainless steels. *Corros.*; 2017, *73*(1), 53-67. https://doi.org/10.5006/2185.
[54] Kölblinger AP, Tavares SSM, Della Rovere CA, & Pimenta AR. Failure analysis of a flange of superduplex stainless steel by preferential corrosion of ferrite phase. Eng. Fail. Anal., 2022, *134*, 106098. https://doi.org/10.1016/j.engfailanal.2022.106098.
[55] Walter NMB, Lemos GVB, Kieckow GS, Buzzatti DT, Buzzatti JT, Mattei F, & Marinho RR. Investigating microstructure, mechanical properties, and pitting corrosion resistance of UNS S32760 super duplex stainless steel after linear friction welding. Journal of Materials Research and Technology, 2024, 31, 1637-1643. https://doi.org/10.1016/j.jmrt.2024.06.191.
[56] Mainier FB, Pegoraro PIF, & Santoro MV. Propargyl alcohol as a corrosion inhibitor for AISI 304L stainless steel in hydrochloric acid. Int. J. Adv. Eng. Res. Sci. (IJAERS), 2018, 5, 168-172. https://dx.doi.org/10.22161/ijaers.5.10.22.
[57] Mainier FB, Farneze HN, Serrão LF, Oliveira BT, & Nani BF. Performance of stainless steel AISI 317L in hydrochloric acid with the addition of propargyl alcohol. International Journal of Electrochemical Science, 2018, 13(4), 3372-3381. https//doi.org/10.20964/2018.04.02.

[58] Askari M, Aliofkhazraei M, & Afroukhteh S. A comprehensive review on internal corrosion and cracking of oil and gas pipelines. Journal of Natural Gas Science and Engineering, 2019, 71, 102971. https://doi.org/10.1016/j.jngse.2019.102971.

[59] Quy Huong D, Duong T, & Nam PC. Effect of the structure and temperature on corrosion inhibition of thiourea derivatives in 1.0 M HCl solution. ACS omega, 2019, 4(11), 14478-14489. https://doi.org/10.1021/acsomega.9b01599.

[60] IUPAC. Periodic Table of Elements. https://iupac.org/what-we-do/periodic-table-of-elements/.

[61] Elayyachy M, El Idrissi A, & Hammouti B. New thio-compounds as corrosion inhibitor for steel in 1 M HCl. *Corrosion Science*, 2006, 48(9), 2470-2479. https://doi.org/10.1016/j.corsci.2005.09.016.

[62] Farsak M, Keleş H. & Keleş M. A new corrosion inhibitor for protection of low carbon steel in HCl solution. *Corrosion Science*, 2015, 98, 223-232. https://doi.org/10.1016/j.corsci.2015.05.036.

[63] ASTM G46-21. American Society of Testing and Materials. Standard guide for examination and evaluation of pitting corrosion, 2021. West Conshohocken, PA.

[64] Örnek C, Långberg M, Evertsson J, Harlow G, Linpé W, Rullik L, & Pan, J. In-situ synchrotron GIXRD study of passive film evolution on duplex stainless steel in corrosive environment. *Corrosion Science*, 2018, 141, 18-21. https://doi.org/10.1016/j.corsci.2018.06.040.

[65] Rahimi E, Kosari A, Hosseinpour S, Davoodi A, Zandbergen H, & Mol JM. Characterization of the passive layer on ferrite and austenite phases of super duplex stainless steel. Applied Surface Science, 2019,496, 143634. https://doi.org/10.1016/j.apsusc.2019.143634.

[66] Agrawal R. & Namboodhiri, TKG. The inhibition of sulphuric acid corrosion of 410 stainless steel by thioureas. *Corrosion Science*, 1990, 30(1), 37-52. https://doi.org/10.1016/0010-938X(90)90233-U.